J. Fluid Mech. (2012), *vol.* 713, *pp.* 453–481. © Cambridge University Press 2012
doi:10.1017/jfm.2012.469

Finite-Péclet-number effects on the scaling exponents of high-order passive scalar structure functions

J. Lepore and L. Mydlarski†

Department of Mechanical Engineering, McGill University, 817 Sherbrooke Street West, Montréal, QC, H3A 0C3, Canada

(Received 23 July 2011; revised 30 August 2012; accepted 20 September 2012; first published online 26 October 2012)

The effect of scalar-field (temperature) boundary conditions on the inertial-convective-range scaling exponents of the high-order passive scalar structure functions is studied in the turbulent, heated wake downstream of a circular cylinder. The temperature field is generated two ways: using (i) a heating element embedded within the cylinder that generates the hydrodynamic wake (thus creating a heated cylinder) and (ii) a mandoline (an array of fine, heated wires) installed downstream of the cylinder. The hydrodynamic field is independent of the scalar-field boundary conditions/injection methods, and the same in both flows. Using the two heat injection mechanisms outlined above, the inertial-convective-range scaling exponents of the high-order passive scalar structure functions were measured. It is observed that the different scalar-field boundary conditions yield significantly different scaling exponents (with the magnitude of the difference increasing with structure function order). Moreover, the exponents obtained from the mandoline experiment are smaller than the analogous exponents from the heated cylinder experiment (both of which exhibit a significant departure from the Kolmogorov prediction). Since the observed deviation from the Kolmogorov $n/3$ prediction arises due to the effects of internal intermittency, the typical interpretation of this result would be that the scalar field downstream of the mandoline is more internally intermittent than that generated by the heated cylinder. However, additional measures of internal intermittency (namely the inertial-convective-range scaling exponents of the mixed, sixth-order, velocity–temperature structure functions and the non-centred autocorrelations of the dissipation rate of scalar variance) suggest that both scalar fields possess similar levels of internal intermittency – a distinctly different conclusion. Examination of the normalized high-order moments reveals that the smaller scaling exponents (of the high-order passive scalar structure functions) obtained for the mandoline experiment arise due to the smaller thermal integral length scale of the flow (i.e. the narrower inertial-convective subrange) and are not solely the result of a more intermittent scalar field. The difference in the passive scalar structure function scaling exponents can therefore be interpreted as an artifact of the different, finite Péclet numbers of the flows under consideration – an effect that is notably less prominent in the other measures of internal intermittency.

Key words: intermittency, turbulent flows, turbulent mixing

† Email address for correspondence: laurent.mydlarski@mcgill.ca

https://doi.org/10.1017/jfm.2012.469 Published online by Cambridge University Press

1. Introduction

A striking property of turbulence is its ability to effectively mix scalar contaminants (such as temperature, salinity, and chemical species) when they are transported within a turbulent flow. Consequently, an understanding of turbulent mixing is crucial to the study of multiple disciplines, including meteorology, oceanic science, combustion, heat transfer and environmental pollutant dispersion. Moreover, a thorough knowledge of the mixing process is essential to the accurate prediction and control of both industrial and environmental flows. A fundamental subset of mixing problems is defined by scalar fields that do not alter the advecting velocity field. Such scalar fields are deemed 'passive' and, given the practical considerations listed above, passive scalar mixing in turbulent flows has been studied extensively, in addition to being reviewed thoroughly by Sreenivasan (1991), Shraiman & Siggia (2000), Warhaft (2000) and Dimotakis (2005).

The predominant theory of turbulence continues to be that of Kolmogorov (1941) (abbreviated as 'K41' herein). K41 theory states that, at high Reynolds numbers ($Re = u'\ell/\nu$, where u' is the root-mean-square (r.m.s.) velocity fluctuation, ℓ is the integral length scale of the turbulence and ν is the kinematic viscosity of the fluid), because there exists a wide range of both length and time scales, the smallest scales of a turbulent flow will be locally homogeneous, isotropic, and, therefore, only a function of the fluid's kinematic viscosity and the dissipation rate of turbulent kinetic energy ($\epsilon \equiv 2\nu\langle s_{ij}s_{ij}\rangle$, where $s_{ij} \equiv (\partial u_i/\partial x_j + \partial u_j/\partial x_i)/2$ is the fluctuating strain rate tensor). Moreover, for an intermediate range of scales, r, such that $\ell \gg r \gg \eta$ (where $\eta \equiv (\nu^3/\epsilon)^{1/4}$ is the Kolmogorov microscale of length), statistics of the flow will also be independent of viscosity. This intermediate range of scales is commonly known as the 'inertial subrange'.

Oboukhov (1949) and Corrsin (1951) extended Kolmogorov theory to the turbulent passive scalar field (commonly referred to as Kolmogorov–Oboukhov–Corrsin, or 'KOC', theory). They analogously argued that, for large Reynolds and Péclet numbers ($Pe = u'\ell_\theta/\alpha$, where ℓ_θ is the scalar integral length scale and α is the scalar diffusivity), there exists an intermediate range of scales, r, referred to as the 'inertial-convective subrange', such that $\ell, \ell_\theta \gg r \gg \eta, \eta_\theta$ (where $\eta_\theta \equiv (\alpha^3/\epsilon)^{1/4}$ is the Corrsin microscale of length for a fluid with a Prandtl number on the order of unity).

While Kolmogorov theory has been shown to be generally valid (especially for low-order statistics, such as the turbulent kinetic energy or scalar variance spectra), the theory has some limitations, with shortcomings of K41/KOC theory being extensively reported; see, for example, Sreenivasan & Antonia (1997) and Warhaft (2000). One noteworthy example is the anomalous scaling of high-order structure functions (of both the velocity and passive scalar fields) in the inertial subrange. Using the passive scalar fluctuations (θ) as an example, the nth-order (longitudinal) structure function is defined as

$$\langle (\Delta_r\theta)^n \rangle \equiv \langle [\theta(x+r) - \theta(x)]^n \rangle, \tag{1.1}$$

where r is a (longitudinal) spatial separation. At high Reynolds and Péclet numbers, passive scalar structure functions exhibit an inertial-convective-range power-law behaviour of the type $\langle (\Delta_r\theta)^n \rangle \sim r^{\xi_n}$, where $\xi_n = n/3$, according to KOC theory. However, it has been shown that the high-order scaling exponents deviate from their predicted values, with the magnitude of the deviation increasing with structure function order.

https://doi.org/10.1017/jfm.2012.469 Published online by Cambridge University Press

The observed departures from K41/KOC theory stem from a phenomenon called internal intermittency. The latter is caused by intense fluctuations in the dissipation rates of turbulent kinetic energy (ϵ) and scalar variance ($\chi \equiv \alpha\langle(\partial\theta/\partial x_i)(\partial\theta/\partial x_i)\rangle$), which are not accounted for in K41/KOC theory. Furthermore, these intense events occur with greater frequency and intensity in the scalar field, when compared to the velocity field (Warhaft 2000). The underlying causes of the stronger intermittency in the passive scalar field remains an active topic of research. An important discovery is that the internal intermittency of passive scalars arises even in non-intermittent velocity fields (Holzer & Siggia 1994; Kraichnan 1994). This 'decoupling' of the passive scalar and velocity fields suggests that the internal intermittency of passive scalars is a result of the mixing process, and not a reflection of the intermittency in the velocity field (Warhaft 2000).

Frisch (1995) defines an intermittent function as one that 'displays activity during only a fraction of the time, which decreases with the scale under consideration'. Consequently, the shape of the probability density function (p.d.f.) of passive scalar increments, which is quasi-Gaussian at large scales, becomes super-Gaussian as one proceeds to progressively smaller scales. Frisch (1995) argued that the kurtosis of the velocity (or scalar) increment (i.e. $\langle(\Delta_r u)^n\rangle$ or $\langle(\Delta_r\theta)^n\rangle$, respectively) will increase without bound as $r \to 0$. Since the kurtosis is a natural measure of the intermittency of a function, the small-scale statistics of the velocity and passive scalar fields are more intermittent than their respective large-scale fields.

One of the most commonly encountered measures of internal intermittency are the inertial-range scaling exponents of the high-order structure functions (or, more precisely, their departure from the K41/KOC theoretical prediction of $n/3$), denoted herein using ζ_n for the velocity field (and ξ_n for the passive scalar field, as previously noted). Velocity structure functions have been measured in a variety of laboratory flows (e.g. Frenkiel & Klebanoff 1967; Antonia, Satyaprakash & Chambers 1982; Anselmet *et al.* 1984; Maurer, Tabeling & Zocchi 1994; Belin, Tabeling & Willaime 1996), atmospheric flows (e.g. Van Atta & Chen 1970; Van Atta & Park 1972; Antonia *et al.* 1982), and numerical simulations (e.g. Vincent & Meneguzzi 1991; Boratav & Pelz 1997; Gotoh, Fukayama & Nakano 2002). The variation of the structure function scaling exponents with structure function order has also received significant theoretical consideration from numerous investigators, including Frisch, Sulem & Nelkin (1978), She & Leveque (1994) and Camussi & Verzicco (2000). See Arneodo *et al.* (1996) for a summary of the velocity structure function scaling exponents obtained in a variety of flows (e.g. jets, grid turbulence, mixing layers, duct flows and cylinder wakes) over a wide range of Reynolds numbers, i.e. $30 \leqslant Re_\lambda \leqslant 5000$.

High-order passive scalar structure functions have also been studied, albeit to a lesser extent. Experimental measurements of ξ_n have been undertaken by Antonia *et al.* (1984), Meneveau *et al.* (1990) and Ruiz-Chavarria, Baudet & Ciliberto (1996), for example. Both Chen & Cao (1997) and Chen & Kraichnan (1998) employed direct numerical simulation of isotropic turbulence to examine the high-order structure functions of the passive scalar field, as well as their inertial-convective-range scaling exponents, whereas Kraichnan (1994) and Lévêque *et al.* (1999) proposed practical models for computing the dependence of the structure function scaling exponents on the structure function order. Of particular interest to the present experiment is the more recent work of Gylfason & Warhaft (2004), Watanabe & Gotoh (2006) and Lepore & Mydlarski (2009).

Gylfason & Warhaft (2004) examined both the longitudinal and transverse temperature structure functions in grid-generated turbulence (for $150 \leqslant Re_\lambda \leqslant 700$)

https://doi.org/10.1017/jfm.2012.469 Published online by Cambridge University Press

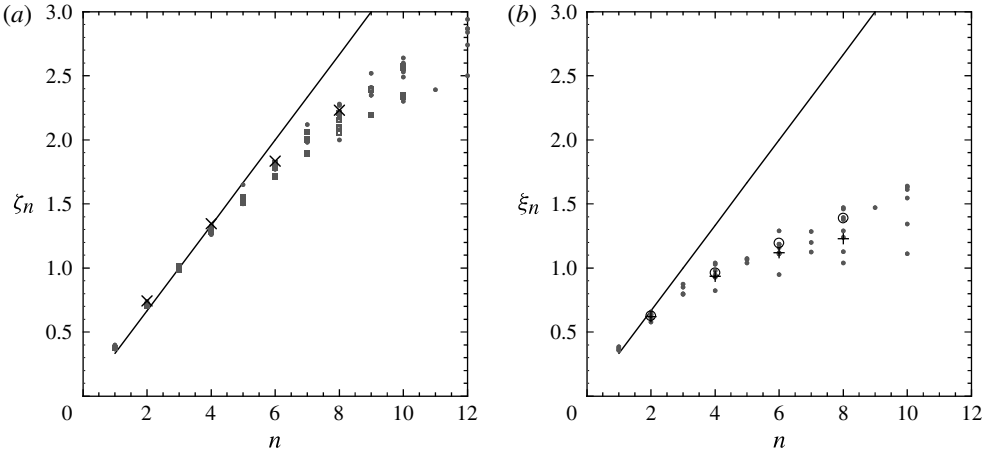


FIGURE 1. The inertial (-convective) range scaling exponents of the (*a*) velocity and (*b*) passive scalar fields, obtained from the published literature. (*a*) ×, present work; •, Anselmet *et al.* (1984), Maurer *et al.* (1994), Belin *et al.* (1996), Vincent & Meneguzzi (1991), Boratav & Pelz (1997), Gotoh *et al.* (2002). Solid line, K41 ($n/3$); □, ESS data of Arneodo *et al.* (1996). (*b*) ○, present work, heated cylinder experiment; +, present work, mandoline experiment; •, Antonia *et al.* (1984), Meneveau *et al.* (1990), Ruiz-Chavarria *et al.* (1996), Gylfason & Warhaft (2004), Chen & Cao (1997), Chen & Kraichnan (1998), Watanabe & Gotoh (2006). Solid line, KOC ($n/3$).

with a uniform mean temperature gradient. They determined that the passive scalar structure function scaling exponents (i) exhibited no dependence on the Reynolds number, and (ii) were the same for both the longitudinal and transverse cases. In addition to their results, they presented a compilation of previously obtained passive scalar scaling exponents, noting that there exists a considerable scatter in the experimentally determined data. Figure 1 presents a compilation of (*a*) velocity and (*b*) temperature scaling exponents. One notices that the velocity scaling exponents exhibit a reasonable collapse at all orders, whereas the passive scalar exponents reveal a considerably larger scatter in the data at high orders. (Note that the data of Maurer *et al.* (1994) and Belin *et al.* (1996) are substantially lower than the remainder of the data presented in figure 1*a*, which are especially close to each other.) Gylfason & Warhaft (2004) noted that the larger scatter in ξ_n could result from (i) convergence issues at high orders, (ii) 'clipping' of large fluctuations due to finite experimental (and computational) domains, and (iii) differences in the initial/boundary conditions of the flow.

Watanabe & Gotoh (2006) examined the high-order passive scalar structure function scaling exponents using high-resolution direct numerical simulations. In particular, their simulations examined an isotropic turbulent flow advecting two different passive scalar fields: (i) a random, Gaussian (white in time) source (at $Re_\lambda = 427$), and (ii) a uniform mean scalar gradient (at $Re_\lambda = 468$). Consistent with the work of Gylfason & Warhaft (2004), they observed that the inertial-range scaling exponents for the longitudinal and transverse structure functions were approximately equal (for the uniform mean scalar gradient experiment). Moreover, their results revealed a significant discrepancy between the scaling exponents generated by the two different scalar sources.

https://doi.org/10.1017/jfm.2012.469 Published online by Cambridge University Press

Motivated by the work of Gylfason & Warhaft (2004), Lepore & Mydlarski (2009) examined the relationship between the high-order passive scalar structure function scaling exponents and the scalar-field boundary conditions at a moderately large Reynolds number ($Re_\lambda = 370$). To explicitly isolate the influence of the scalar-field boundary conditions, they devised an experimental apparatus that could inject the scalar (temperature) field using two different heat injection methods, without altering the advecting velocity field. They found that the high-order passive scalar structure function scaling exponents were sensitive to the scalar-field boundary conditions, thereby experimentally confirming the direct numerical simulations of Watanabe & Gotoh (2006). Moreover, given the finite Reynolds numbers of experimental and simulated flows, their results revealed that previous estimates of the inertial-convective-range scaling exponents of the passive scalar structure functions are subject to the boundary conditions of the scalar field and can therefore not be considered as universal, as previously noted when comparing ζ_n for boundary layers and other flows (e.g. Arneodo *et al.* 1996).

The results of Watanabe & Gotoh (2006) and Lepore & Mydlarski (2009) potentially cast doubt on the universality of small-scale passive scalars, and, in particular, whether the structure function scaling exponents are in fact independent of the scalar-field boundary conditions. Given that structure function scaling exponents are frequently employed as a measure of the internal intermittency, the objective of the present work is to investigate their sensitivity to the scalar-field boundary conditions. Moreover, the current research attempts to explain the observed behaviour of the passive scalar structure function scaling exponents. This is accomplished by using two different, large-scale heat injection methods in two flows which are otherwise hydrodynamically identical.

The remainder of this paper is organized as follows: the experimental apparatus is presented in § 2. Results are presented and discussed in § 3, which examines (i) different measures of internal intermittency, (ii) finite-Péclet-number effects, and (iii) compensation of normalized structure functions (to account for the previous effects). Our conclusions are summarized in § 4. The Appendix characterizes the hydrodynamic and thermal fields examined in the present experiment, and follows § 4.

2. Apparatus

The experiments described herein were conducted in the open-circuit, suction-design, low-background-turbulence wind tunnel located in the Aerodynamics Laboratory at McGill University. The experimental facility is the same as that employed by Beaulac & Mydlarski (2004), Lepore & Mydlarski (2009) and Berajeklian & Mydlarski (2011). The details of the tunnel's construction are described therein.

In the present work, the flow under consideration is the turbulent wake downstream of a circular cylinder. To generate the hydrodynamic wake, a circular cylinder (of diameter $D = 73.0$ mm) was installed at the entrance of the tunnel test section and placed in a uniform flow (U_∞) of 10.3 m s^{-1}. (It was oriented vertically and spanned the entire extent of the test section.) Consequently, the Reynolds number of the flow ($Re_D = U_\infty D/\nu$) is $Re_D = 47\,900$. To inject the scalar (temperature) into the flow, a 1.5 kW electric heating element was installed within the cylinder. Energizing the heating element yields a 'heated cylinder', which was one of the two methods for injecting the scalar into the flow field. The other required a 'mandoline' to be installed 10 diameters downstream of, and oriented parallel to, the cylinder (see figure 2). First introduced by Warhaft & Lumley (1978), the mandoline consists of an array of fine

https://doi.org/10.1017/jfm.2012.469 Published online by Cambridge University Press

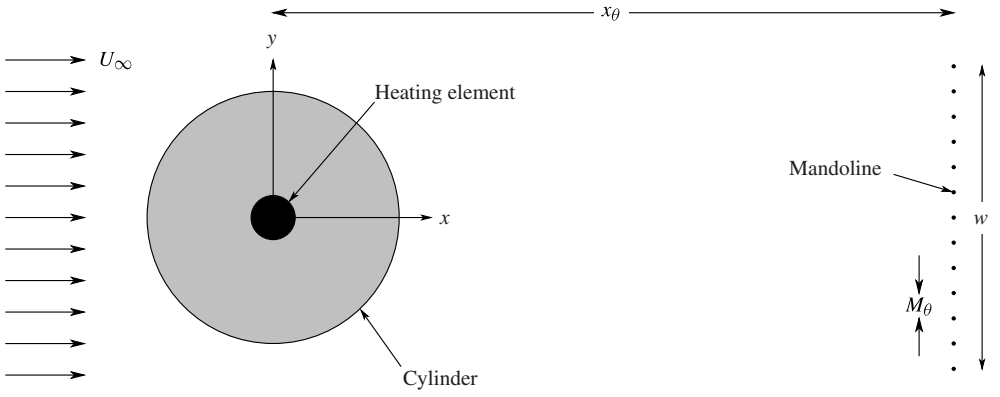


FIGURE 2. Schematic illustrating the experimental configuration. A heating element is embedded within the cylinder that generates the hydrodynamic wake (thus creating a 'heated cylinder'). In addition, a 'mandoline' is installed downstream of the cylinder. Consequently, one can employ either the heated cylinder or the mandoline to generate the thermal wake. In either case, the hydrodynamic flow field remains unchanged. The hot- and cold-wire sensors are located 30 diameters downstream of the cylinder and along its axis (corresponding to non-dimensional coordinates of $x/D = 30$ and $y/D = 0$). In the current research $x_\theta/D = 10$.

Nichrome wires that are stretched across the wind tunnel test section. When energized (using a DC power supply capable of providing 1.2 kW), the individual plumes of the multiple wires grow and rapidly mix, thus providing a second method of heating the wake. To prevent the wires from sagging when heated, small springs are attached to one end of each wire to keep them in tension. In the current configuration, thirteen 36 AWG (0.127 mm in diameter) wires were employed, evenly spaced 7.6 mm apart (yielding a total mandoline width of 91.4 mm. Moreover, given the small size of the individual wires, the presence of the mandoline does not disturb the hydrodynamic field (see the Appendix). In particular, one may examine the Reynolds number of the flow past the wire to determine whether vortices are being shed from the wire. As a worst-case estimate, one can assume that the velocity of the flow past the wire is U_∞ (thus yielding an over-estimate of the wire Reynolds number). Using the heat transfer correlation proposed by Zukauskas (1972), the surface temperature of the wire, and therefore the film temperature of the flow, can be estimated, and the kinematic viscosity of the fluid determined. The resulting Reynolds number, $Re_{source} = U_\infty D_{source}/\nu$ (where D_{source} is the diameter of the Nichrome wire), yields a value of 47, which is slightly larger than the critical value of 40 for vortex shedding. Given that the flow exhibits none of the phenomena associated with vortex shedding (i.e. no spikes are present in the velocity spectra: see figure 11c), one may conclude that the effects of vortex shedding, if at all present, are small (especially when compared to the effects of the turbulence). Therefore, the presence of the mandoline did not alter the velocity field, and consequently the velocity field was the same when either scalar injection mechanism was used.

The turbulent velocity field and the fluctuating temperature field were measured simultaneously by means of hot-wire anemometry and cold-wire thermometry, respectively. The hot-wire sensor, consisting of a 3 μm diameter tungsten wire with a sensing length of approximately 0.5 mm (yielding a length-to-diameter ratio of 200), was mounted beside a 0.625 μm diameter and 0.5 mm long platinum-10 % rhodium

https://doi.org/10.1017/jfm.2012.469 Published online by Cambridge University Press

cold-wire on a TSI 1244 parallel-sensor probe. The hot-wire was operated at an overheat of 1.8 using a TSI IFA 300 constant temperature anemometer, whereas the cold-wire sensor was supplied with a constant current of 100 μA from a custom-built, cold-wire thermometer constructed at the Université Laval (Québec, Canada). It was based on the constant-current anemometry circuit of Lemay & Benaïssa (2001). Given the variable-temperature flow under consideration herein, the calibration of the hot-wire sensors employed a King's law relationship with temperature-dependent coefficients, as described in Lienhard & Helland (1989). The sensors were calibrated in a (laminar) TSI 1127 calibration jet that was modified to include the addition of electric heaters to heat the upstream air supply to enable variable-temperature calibrations. When operated in a flow of approximately 10 m s^{-1}, LaRue, Deaton & Gibson (1975) determined that the −3 dB point of the frequency response of a 0.63 μm diameter platinum cold wire is ∼6.3 kHz. Given that the Kolmogorov frequencies of the flows studied herein are roughly 7 kHz, the temporal resolution of the cold-wire is satisfactory, and a correction, such as that proposed by Lemay & Benaïssa (2001), was not required (in addition to being found to distort some higher-order temperature statistics). The hot- and cold-wire sensors are located 30 cylinder diameters downstream of the cylinder and along the cylinder's axis ($x/D = 30$ and $y/D = 0$, respectively). The sensors are mounted on a precision-stepper-motor-controlled traversing mechanism to permit the measurement of transverse profiles of the wake. At the measurement location specified above, the Taylor microscale Reynolds number ($Re_\lambda \equiv u'\lambda/\nu$, where $\lambda \equiv \sqrt{\langle u^2\rangle/\langle(\partial u/\partial x)^2\rangle}$ is the Taylor microscale of length) is 370. The relevant flow parameters are summarized in table 1.

The output signals of the hot-wire anemometer and cold-wire thermometer were high-pass filtered at 0.1 Hz, low-pass filtered at 12 and 6 kHz (respectively) and amplified using a Krohn-Hite 3384 filter. The filtered signals were then digitized and stored for future data reduction using a 16-bit National Instruments PCI 6143 simultaneous-sampling multifunction data acquisition card. The simultaneous velocity–temperature data were sampled at twice the low-pass filter frequency (in accordance with the Nyquist criterion) using 5000 blocks of 16 384 samples per block, yielding a time-series data set consisting of 8.192×10^7 samples. In addition to the velocity–temperature data, additional measurements of (only) the temperature field were obtained using only the cold-wire. The second data set consisted of 7500 blocks of 16 834 samples (for a total of 1.2288×10^8 samples), once again recorded at twice the low-pass filter frequency. Consequently, the total sampling time for the simultaneous velocity–temperature and individual temperature data sets was 58 and 87 min, respectively.

3. Results and discussion

The following section is divided into three subsections. The first examines different (previously proposed) measures of internal intermittency, including results pertaining to the (i) high-order passive scalar structure functions (and their inertial-convective-range scaling exponents, as discussed in Lepore & Mydlarski 2009), (ii) mixed sixth-order velocity–temperature structure functions, and (iii) (non-centred) autocorrelations of the dissipation rate of scalar variance. The second discusses the sensitivity of the previous results to the scalar-field boundary conditions (or, more precisely, the finite Péclet numbers of the flows under consideration). In this context, the normalized high-order moments of passive scalar increments are of particular interest. The final subsection

https://doi.org/10.1017/jfm.2012.469 Published online by Cambridge University Press

U_∞ (m s^{-1})	10.3	
$Re_D\{\equiv U_\infty D/\nu\}$	47 900	
$Re_\lambda\{\equiv u'\lambda/\nu\}$	370	
$\langle U\rangle$ (m s^{-1})	8.42	
u' (m s^{-1})	1.01	
$\epsilon\{=15\nu\left\langle(\partial u/\partial x)^2\right\rangle\}$ (m^2 s^{-3})	6.85	
$\ell\{=\int_0^\infty \rho_{uu}(r)\,\mathrm{d}r\}$ (mm)	280	
$\lambda\{=\sqrt{\left\langle u^2\right\rangle/\left\langle(\partial u/\partial x)^2\right\rangle}\}$ (mm)	5.95	
$\eta\{\equiv(\nu^3/\epsilon)^{1/4}\}$ (mm)	0.154	
$Re\{=u'\ell/\nu\}$	18 100	
	Heated cylinder	Mandoline
θ' (K)	0.195	0.164
$K_\theta\{=\left\langle\theta^4\right\rangle/\left\langle\theta^2\right\rangle^2\}$	3.44	2.86
$SK_\theta\{=\left\langle\theta^6\right\rangle/\left\langle\theta^2\right\rangle^3\}$	26.1	14.1
$HK_\theta\{=\left\langle\theta^8\right\rangle/\left\langle\theta^2\right\rangle^4\}$	422	112
$\chi\{=3\alpha\left\langle(\partial\theta/\partial x)^2\right\rangle\}$ (K^2 s^{-1})	0.115	0.119
$\ell_\theta\{=\int_0^\infty \rho_{\theta\theta}(r)\,\mathrm{d}r\}$ (mm)	314	105
$\lambda_\theta\{=\sqrt{\left\langle\theta^2\right\rangle/\left\langle(\partial\theta/\partial x)^2\right\rangle}\}$ (mm)	4.68	3.88
$\eta_\theta\{\equiv(\alpha^3/\epsilon)^{1/4}\}$ (mm)	0.199	0.199
$Pe\{=u'\ell_\theta/\alpha\}$	14 700	4900

TABLE 1. Flow parameters. Fluid properties are evaluated at 298K ($\nu = 15.7\times 10^{-6}$ m^2 s^{-1}, $\alpha = 22.2\times 10^{-6}$ m^2 s^{-1}). $D = 73.0$ mm is the cylinder diameter. Note that the experiments described herein were performed at a downstream location of $x/D = 30$ and a transverse position of $y/D = 0$. Please refer to the schematic presented in figure 2 for the location and orientation of the coordinate axes.

attempts to compensate the aforementioned normalized high-order moments to obtain further insight into the influence of the large scales of the scalar field.

3.1. *Measures of internal intermittency*

Figure 3 plots the even-order structure functions (up to order $n = 8$) of the temperature field, non-dimensionalized using Kolmogorov variables. (To avoid the introduction of any artifacts, the structure functions are computed using the raw difference, as opposed to using their absolute value. Hence, the odd-order moments are not presented.) One observes that, at second order, the structure functions obtained using the different heat injection mechanisms are indistinguishable in the inertial-convective and dissipative ranges, consistent with KOC theory. However, as the order increases, one observes that the structure functions begin to deviate at progressively smaller scales – the sixth-order structure functions begin to deviate in the inertial-convective range whereas the eighth-order structure functions are different for a large range of scales. The implication is that the effects of the scalar-field boundary conditions permeate to progressively smaller scales as the structure function order increases (Lepore & Mydlarski 2009).

https://doi.org/10.1017/jfm.2012.469 Published online by Cambridge University Press

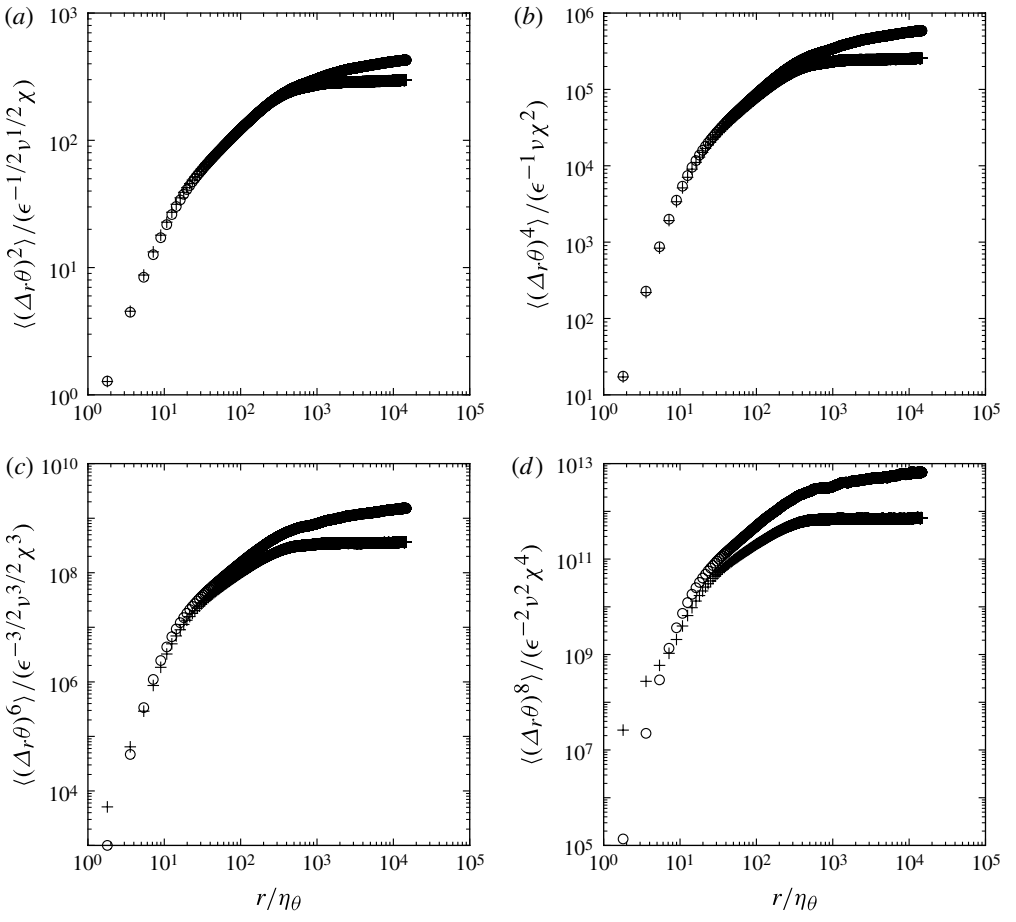


FIGURE 3. The nth-order structure functions of the temperature increment, normalized using Kolmogorov variables. (*a*) $n = 2$; (*b*) $n = 4$; (*c*) $n = 6$; (*d*) $n = 8$. ∘, heated cylinder; +, mandoline. Note that the above data also appear in Lepore & Mydlarski (2009).

Since the current work examines the inertial-convective-range scaling exponents of the high-order passive scalar structure functions, one must objectively determine the extent of the inertial-convective range, so that its scaling can be systematically estimated. The former is accomplished using 'Yaglom's 4/3 law' (Yaglom 1949), which states that, for large Reynolds and Péclet numbers,

$$\langle(\Delta_r u)\ (\Delta_r\theta)^2\rangle = -\tfrac{4}{3}\chi r, \tag{3.1}$$

in the inertial-convective range. This is analogous to the procedure used in Anselmet *et al.* (1984). Therein, the authors employ Kolmogorov's 4/5 law, for which $\langle(\Delta_r u)^3\rangle = -4\epsilon r/5$ in the inertial range. They argued in favour of using the third-order velocity structure function to determine the extent of the inertial range, given that it is the only structure function in which its inertial range is unaffected by internal intermittency. The same argument holds for the mixed third-order structure function examined herein. The extent of the inertial-convective range is established by determining the two separations at which the compensated mixed third-order structure

https://doi.org/10.1017/jfm.2012.469 Published online by Cambridge University Press

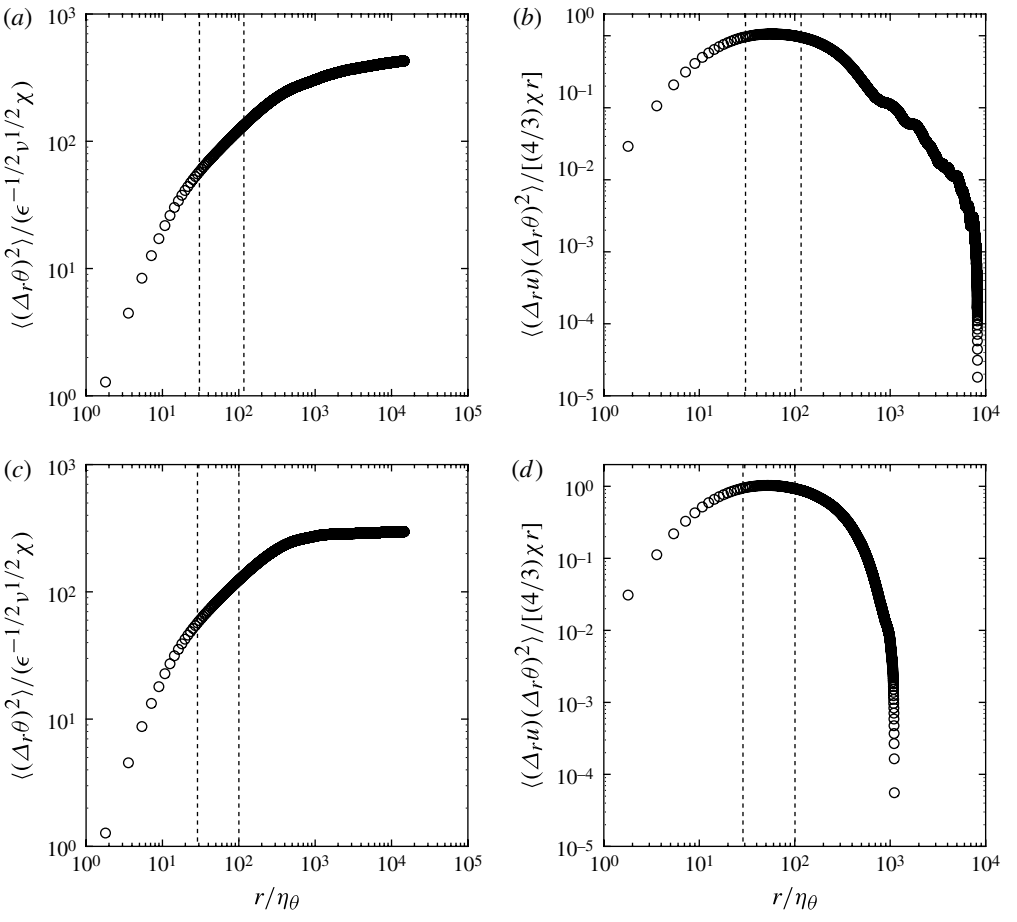


FIGURE 4. The second-order and mixed third-order structure functions of the temperature fluctuation, subject to varying scalar-field boundary conditions. (*a*,*c*) Second-order structure function (non-dimensionalized using Kolmogorov variables); (*b*,*d*) mixed third-order structure function (normalized according to the Yaglom 4/3 law to determine the extent of the inertial-convective range). (*a*,*b*) Heated cylinder; (*c*,*d*) mandoline. In all figures, the dashed lines denote the upper and lower bounds of the inertial-convective-range scaling region (defined as the separations corresponding to the locations at which the compensated mixed third-order structure function falls to 90 % of its maximum value).

function falls to 90 % of its maximum value, in a manner analogous to that of Jayesh, Tong & Warhaft (1994). Figure 4 presents both the second-order structure function of the temperature fluctuations and the mixed third-order structure function, generated using either the heated cylinder or the mandoline. In figure 4, the upper and lower bounds of the inertial-convective range, as defined above, are represented by the dashed lines. (Note that the different scalar injection methods yield different inertial-convective ranges.) One observes that this region corresponds to the power-law region exhibited in the second-order temperature structure functions (figures 4*a* and 4*c*), as expected. Consequently, the technique outlined above is employed herein as a consistent method for determining the limits of the inertial range.

https://doi.org/10.1017/jfm.2012.469 Published online by Cambridge University Press

Given the difficulties associated with identifying the extent of the inertial range, Benzi *et al.* (1993) proposed an alternative technique for determining the velocity structure function scaling exponents; see also Benzi *et al.* (1995). By plotting the high-order structure functions versus the third-order structure function (as opposed to the separation, r), Benzi *et al.* (1993) discovered that the inertial-range scaling region was significantly extended, especially in low-Reynolds-number flows – a phenomenon they refer to as 'extended self-similarity' (ESS). However, ESS is not without its limitations. Firstly, ESS yields relative scaling exponents, since the structure functions are plotted versus the third-order structure function, which only scales as r in the limit of infinite Reynolds numbers; see, for example, Mydlarski & Warhaft (1996) for the dependence of the third-order structure function on Reynolds number. Furthermore, Stolovitzky & Sreenivasan (1993) discovered that the extended scaling range is not observed in higher-order moments. More precisely, the eighth-order moments examined therein exhibited two distinct scaling regions for the dissipative and inertial ranges. Stolovitzky & Sreenivasan (1993) thus concluded that ESS is only valid for the low-order statistics. (Note that Benzi *et al.* 1993 only present structure functions up to sixth order.) A similar conclusion regarding ESS was also drawn by Anselmet, Antonia & Danaila (2001), who observed an 'inflectional behaviour' in the ESS-compensated data with increasing structure function order, especially at high Reynolds numbers. In addition, Chen & Cao (1997) encountered some difficulty in estimating the errors bars for their ESS-calculated structure function scaling exponents, noting that '[t]he error bar for the extracted scaling exponents in the inertial range seems bigger than the result using the original structure functions'.

Despite the aforementioned limitations, Ruiz Chavarria, Baudet & Ciliberto (1995) proposed an analogous ESS technique for the passive scalar field. Intuition would suggest plotting the scalar structure functions versus the mixed third-order structure function, $\langle(\Delta_r u)\,(\Delta_r\theta)^2\rangle$ (given the analogy between Kolmogorov's 4/5 law and Yaglom's 4/3 law, both of which are proportional to r in the inertial(-convective) range). However, Ruiz Chavarria *et al.* (1995) chose to use the second-order structure function instead. Consequently, one must also determine the second-order scaling exponent to determine higher-order scaling exponents. (Otherwise, one can only compute the relative scaling exponents, ξ_n/ξ_2.) This complicates the analysis, since one cannot assume that the second-order structure function will scale as $r^{2/3}$. (As demonstrated in the compilation presented in figure 1*b* in the present work, the experimentally determined values of ξ_2 vary from 0.58 to 0.66.) That being said, neither can one assume that $\langle(\Delta_r u)\,(\Delta_r\theta)^2\rangle$ scales as r in the inertial-convective subrange for non-infinite Reynolds and Péclet numbers (Mydlarski & Warhaft 1998). Furthermore, upon examination of figure 3 of Ruiz Chavarria *et al.* (1995), one clearly observes that this technique does not enhance the inertial-convective scaling region (this is especially true at higher orders: see their figure 3*b*). Therefore, given the significant difficulties presented above, the present work does not make use of ESS to compute the structure function scaling exponents.

The structure function scaling exponents were determined by fitting a least-squares power-law curve fit to the data in the inertial-convective range, defined using the previously described method. The scaling exponents for the passive scalar field are plotted in figure 1(*b*) (and listed in table 2). When compared with the results of the other researchers in figure 1(*b*), one observes that they fall within the range of exponents in the published literature. Moreover, the current results for the scalar field generated using the mandoline agree well with the exponents presented in Ruiz-Chavarria *et al.* (1996) (albeit estimated by ESS), whose experimental configuration

https://doi.org/10.1017/jfm.2012.469 Published online by Cambridge University Press

n	ζ_n	ξ_n Heated cylinder	ξ_n Mandoline
2	0.74	0.63 ± 0.005	0.62 ± 0.005
4	1.35	0.96 ± 0.01	0.93 ± 0.01
6	1.83	1.19 ± 0.01	1.12 ± 0.02
8	2.23	1.39 ± 0.02	1.23 ± 0.03

TABLE 2. The inertial-range scaling exponents of the structure functions of the velocity (ζ_n) and passive scalar (ξ_n) fields. Note that the values listed in the table above are the averages obtained from multiple experiments. The error bars represent the maximum deviation from the average value observed for the different experiments.

closely resembled the mandoline experiment studied herein. More importantly, one immediately notices that the passive scalar structure function scaling exponents for the two different scalar-field boundary conditions (i) deviate substantially from the KOC $n/3$ theoretical prediction, and (ii) are significantly different from each other at high orders, thus indicating a dependence of the high-order statistics on the scalar-field boundary conditions. (Note that the velocity structure function scaling exponents were also computed using the different scalar-field boundary conditions. At eighth order, the velocity scaling exponents differed by approximately 1 %, which is considerably smaller than the 13 % difference observed in the passive scalar exponents, thereby confirming that the observed discrepancy in the passive scalar exponents is not a spurious result of any differences in the velocity fields: see the Appendix.) Given the moderately high Reynolds number of the flow examined herein, the present results imply a dependence of the small-scale passive scalar field on the large scales. However, Kolmogorov theory is only posed in the limit of infinite Reynolds (and Péclet) numbers. Therefore, the observed discrepancy in the scaling exponents could be an artifact of the non-infinite Reynolds number of the flow. Nevertheless, as concluded in Lepore & Mydlarski (2009), the present work reveals that all previous estimates of the passive scalar structure function scaling exponents (because they are all measured/calculated in finite-Reynolds-number flows) are subject to the scalar-field boundary conditions. The question of Reynolds (or, more precisely, Péclet) number dependences will be addressed in the next subsection.

In comparing the scaling exponents measured herein with the KOC $n/3$ prediction, one observes that the scalar field generated using the mandoline exhibits scaling exponents that are smaller than those measured in the temperature field generated by heating the cylinder. Since the deviation from Kolmogorov theory results from internal intermittency effects, the magnitude of this departure from KOC is frequently used as a measure of the intermittency. Consequently, the scaling exponents presented in table 2 imply that the scalar field generated by the mandoline is more intermittent than that generated by the heated cylinder. Furthermore, the current results demonstrate that the passive scalar structure function scaling exponents are sensitive to the large-scale features of the flow, i.e. the scalar-field boundary conditions. It is therefore of interest to determine if alternate statistics can be used to provide insight into the small-scale structure of the passive scalar field.

To this end, the (i) sixth-order, mixed (velocity–temperature) structure functions, $\langle(\Delta_r u)^2\,(\Delta_r\theta)^4\rangle$, and (ii) (non-centred) autocorrelations of the dissipation rate of scalar variance, $\rho_{\chi\chi}(r) \equiv \langle\chi(x)\chi(x+r)\rangle/\langle\chi^2\rangle$, were also obtained for each of the two flows:

https://doi.org/10.1017/jfm.2012.469 Published online by Cambridge University Press

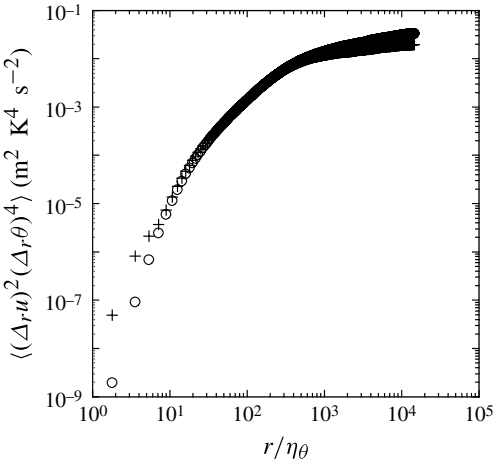


FIGURE 5. The mixed sixth-order structure function, $\langle(\Delta_r u)^2\,(\Delta_r\theta)^4\rangle$, plotted as a function of the non-dimensional separation, obtained using the different scalar-field boundary conditions: ∘, heated cylinder experiment; +, mandoline experiment.

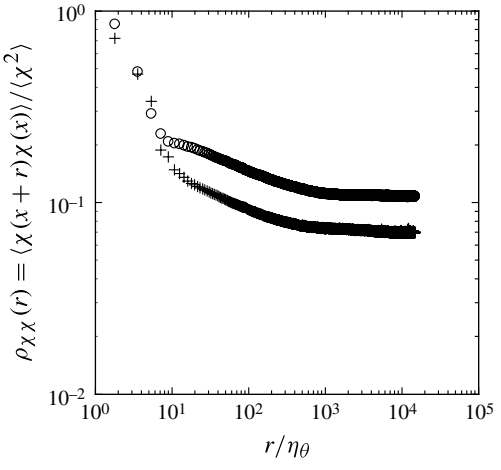


FIGURE 6. The non-centred autocorrelation of the dissipation rate of scalar variance, $\rho_{\chi\chi}(r)$, plotted as a function of the non-dimensional separation, obtained using the different scalar-field boundary conditions: ∘, heated cylinder experiment; +, mandoline experiment.

see figures 5 and 6, respectively. In the inertial-convective scaling range, the former scales as $r^{2-\mu_\theta}$, whereas the latter scales as $r^{-\mu_\theta}$, where μ_θ is the scalar intermittency exponent and can be used to quantify the degree of internal intermittency; see for example Antonia *et al.* (1984) or Warhaft (2000). Consequently, these additional statistics can also be used to obtain quantitative estimates of the internal intermittency of the passive scalar fields examined herein.

Figure 5 reveals that the scalings of the sixth-order, mixed velocity–temperature structure functions for the scalar fields generated by the heated cylinder and the mandoline are quite similar – much more so than the analogous plots of the sixth-

https://doi.org/10.1017/jfm.2012.469 Published online by Cambridge University Press

order passive-scalar structure function (see figure 3*c*). This similarity is quantitatively confirmed by the inertial-convective-range scaling exponents for these two figures (measured in the same manner as for the passive scalar structure functions), which are 1.638 and 1.644 for the heated cylinder and mandoline experiments, respectively.

To place these exponents in the context of previous research, we note that Chambers & Antonia (1984) measured (by means of structure function compensation) the scaling exponents of $\langle(\Delta_r u)^2\,(\Delta_r\theta)^4\rangle$ to be 1.75 ± 0.05 in the atmospheric surface layer, whereas Schmitt *et al.* (1996) obtained 1.65 ± 0.05 (also in the atmospheric surface layer) using least-squares regression in the inertial range. In the wake of a heated cylinder, Lévêque *et al.* (1999) obtained a scaling exponent of 1.608 ± 0.028 using ESS. Xu, Antonia & Rajagopalan (2000) measured, by least-squares regression, the scaling exponent to be 1.83 in a turbulent round jet. At the highest Reynolds number in active-grid turbulence, Mydlarski (2003) measured the scaling exponent to be 1.52 ± 0.05 (by means of structure function compensation) and 1.58 (using ESS). Boratav & Pelz (1998) estimated the scaling exponents in their DNS of homogeneous, isotropic turbulence by means of ESS and found them to be 1.61 ± 0.04. Consequently, the current results fall within the range of the values observed in the literature. Moreover, the current measurements imply that the estimates of μ_θ for both scalar fields are approximately 0.36. This result is especially consistent with the results of both Sreenivasan, Antonia & Danh (1977) and Prasad, Meneveau & Sreenivasan (1988), who estimate $\mu_\theta \approx 0.35$ and 0.38, respectively. Chambers & Antonia (1984) found $\mu_\theta = 0.25 \pm 0.05$, whereas Mydlarski & Warhaft (1998) found $0.19 \leqslant \mu_\theta \leqslant 0.28$ over a range of Reynolds numbers. In the context of the present work, the precise value of μ_θ is not as important as the fact that both estimates of μ_θ are effectively identical for the two different scalar fields. (It has been demonstrated that the different approaches used to calculate the intermittency exponents can result in different estimates: see Sreenivasan & Kailasnath 1993 and Mydlarski 2003.)

Alternately, μ_θ is found to be 0.172 and 0.176 for the scalar fields generated by the heated cylinder and mandoline, respectively, when calculated from the (non-centred) autocorrelations of the dissipation rates of scalar variance, $\rho_{\chi\chi}(r)$: see figure 6. Once again, both values are effectively identical, thus implying that the passive scalar fields generated by both the heated cylinder and the mandoline exhibit similar levels of internal intermittency. (The reason that the two autocorrelations have different, non-zero, large-scale asymptotes is that these are non-centred autocorrelations – as opposed to centred ones – with different scalar dissipation statistics. As was shown in Mydlarski & Warhaft (1996, p. 363), an equation can be derived which gives the value of the asymptote as a function of the square of the mean dissipation and the variance of the dissipation.)

Lastly, we remark that, by use of an intermittency model, μ_θ can also be inferred from the measured values of ξ_n. The model of Cao & Chen (1997) was used herein to estimate the intermittency exponents by applying a least-squares curve fit to the scaling exponent data presented in table 2. (Note that the model assumes that the intermittency exponent for the velocity field, μ, which is the same for both flows, is $\mu = 2/9 = 0.22$.) The resulting inferred scalar intermittency exponents were $\mu_\theta = 0.246$ and 0.288 for the heated cylinder and mandoline experiments, respectively. These estimates differ by 17 % – at least one order of magnitude larger than the difference obtained when comparing the intermittency exponents computed from the mixed sixth-order structure functions and the autocorrelations of χ. Consequently, this result reinforces the significance of the perceived difference

https://doi.org/10.1017/jfm.2012.469 Published online by Cambridge University Press

in internal intermittency when using higher-order passive scalar structure function exponents as a measure, given that the values of μ_θ (and therefore the degrees of passive scalar internal intermittency) determined from both the sixth-order, mixed velocity–temperature structure functions and the autocorrelations of χ can be considered to be experimentally indistinguishable.

3.2. *Finite-Péclet-number effects*

In addition to the statistics described above, it is useful to consider the higher-order moments of the passive scalar increments (as a function of the separation, r), normalized by the second-order structure function. Normalized fourth-, sixth- and eighth-order passive scalar structure functions are presented in figure 7(*a–c*). (These will be referred to herein as the kurtosis, super-kurtosis and hyper-kurtosis structure functions, respectively.) One observes that, at large scales, the curves roughly asymptote to their respective Gaussian values (3, 15 and 105). More precisely, the heated cylinder data appear to asymptote to a value that is slightly larger than the analogous value for the mandoline experiment. This result is not unreasonable since the kurtosis of the scalar fluctuations (i.e. K_θ) is larger for the heated cylinder experiment: see table 1. (One can easily demonstrate that, in the limit of $r \to \infty$, $K_{\Delta_r\theta} \to K_\theta$.) At small scales, one notices significant departures from the Gaussian prediction, due to the effects of internal intermittency.

Significantly, one also observes that, for all three subfigures, the mandoline data achieve Gaussian values at smaller scales than do the heated cylinder data. For example, the mandoline data clearly attain their large-scale value ($\sim$15) for the super-kurtosis (i.e. figure 7*b*) at roughly $r/\eta_\theta \approx 10^3$, whereas the heated cylinder data only do so towards the end of the recorded data ($r/\eta_\theta \approx 10^4$), or even beyond that. This occurs because the thermal integral length scale for the mandoline experiment is smaller than the corresponding value for the heated cylinder experiment. (Table 1 indicates that $\ell_\theta = 105$ and 314 mm for the mandoline and heated cylinder experiments, respectively.) This effect spuriously steepens the inertial-convective-range slope of the mandoline super-kurtosis structure function (making it more negative, due to the smaller scalar integral length scale/smaller Péclet number) relative to that of the heated cylinder experiment because it must fall from its small-scale value (at $r \to 0$) to its large-scale value (at $r \approx \ell_\theta$) over a smaller range of scales.

As an aside, it is worth noting that one might be tempted to extrapolate this argument to conclude that the scaling exponents, ξ_n, will tend to increase with Reynolds/Péclet number, and potentially asymptote to $n/3$. However, such an argument in incorrect because it neglects to include the fact that intermittency effects also increase with Reynolds number, as does the width of the inertial-convective range. For example, the kurtosis of $\partial u/\partial x$, or equivalently $\partial\theta/\partial x$, increases with Reynolds/Péclet number (e.g. Sreenivasan & Antonia 1997). Such an argument is akin to stating that the (fourth-order) kurtosis structure functions asymptote to 3 at all scales as $Re \to \infty$. However, the tendency for this to occur (due to the increase in extent of the scaling range) is offset by the increase in $K_{\partial\theta/\partial x}$ with Reynolds number.

Returning to the arguments at hand, note that the inertial-convective-range scaling exponents of the normalized higher-order moments of the passive scalar increments (denoted by γ_n) can be related to the structure function scaling exponents (ξ_n) as

$$\gamma_n \equiv \xi_n - \left(\frac{n}{2}\right)\xi_2, \tag{3.2}$$

https://doi.org/10.1017/jfm.2012.469 Published online by Cambridge University Press

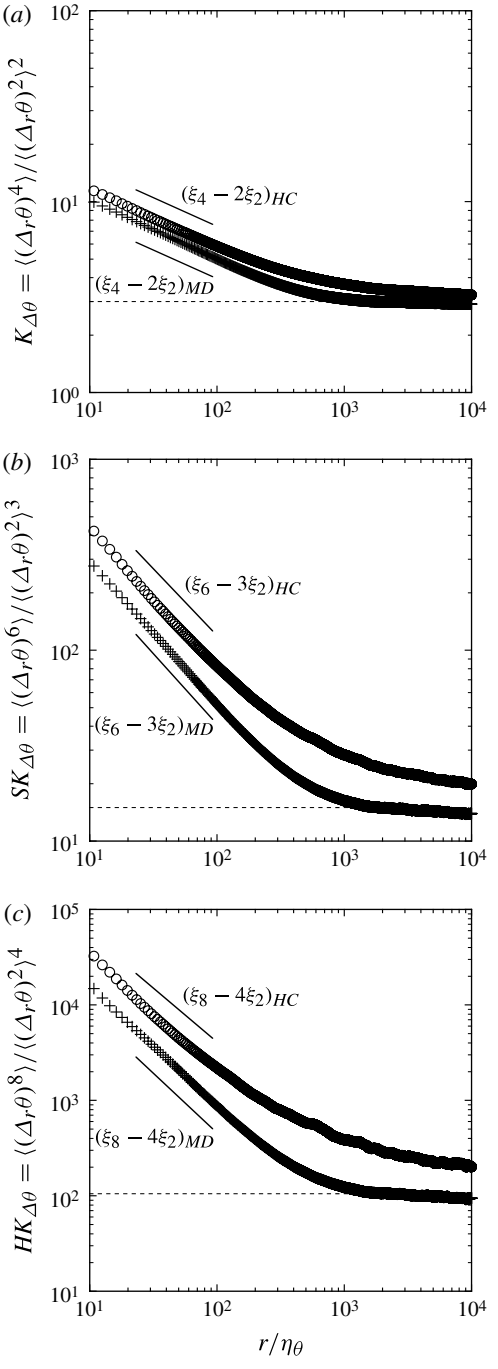


FIGURE 7. The high-order moments of the passive scalar increments, $\langle(\Delta_r\theta)^n\rangle/\langle(\Delta_r\theta)^2\rangle^{n/2}$, plotted as a function of the separation (r/η_θ). (*a*) Kurtosis ($n = 4$); (*b*) super-kurtosis ($n = 6$); (*c*) hyper-kurtosis ($n = 8$). ∘, heated cylinder experiment; +, mandoline experiment. The dashed line corresponds to the Gaussian prediction.

https://doi.org/10.1017/jfm.2012.469 Published online by Cambridge University Press

because, in the inertial-convective range,

$$\langle(\Delta_r\theta)^n\rangle/\left\langle(\Delta_r\theta)^2\right\rangle^{n/2} \propto r^{\gamma_n} = r^{\xi_n}/(r^{\xi_2})^{n/2} = r^{\xi_n-(n/2)\xi_2}. \tag{3.3}$$

As demonstrated in table 2, the second-order structure function scaling exponents are experimentally indistinguishable for the heated cylinder and mandoline experiments. Consequently, the slopes of the normalized high-order moments (γ_n) are directly related to the inertial-convective-range scaling exponents of the passive scalar structure functions of the same order (ξ_n). Since we have already demonstrated that γ_n for the mandoline is smaller than that of the heated cylinder (due to the smaller thermal integral length scale/narrower inertial-convective range), one may therefore conclude that the structure function scaling exponents (ξ_n) for the scalar field generated by the mandoline are smaller than the corresponding values for the heated cylinder for the same reason, and are not uniquely the result of a more intermittent passive scalar field.

The dependence of the scaling exponents (either ξ_n or γ_n) on ℓ_θ (and therefore on the width of the inertial-convective range, since the two scalar fields have identical Corrsin microscales of length, η_θ: see table 1) is, in effect, a Péclet number dependence. Recall that the Péclet number should be defined as $Pe = u'\ell_\theta/\alpha$, since the integral scale of the scalar field, ℓ_θ, is different from that of the velocity field, ℓ. Therefore, it is incorrect to simply write $Pe = Re \times Pr$, where Pr is the Prandtl number of the fluid, since such an (overly simple) expression for the Péclet number would yield the same value for both scalar fields, which is not the case herein, given that both scalar fields have different integral length scales.

To account for this Péclet-number dependence, one may normalize the data in figure 7 in a manner that compensates for this effect. More precisely, the spatial separation r is non-dimensionalized using the integral length scale of the passive scalar field: $[(r/2\pi) - \eta_\theta]/[\ell_\theta - \eta_\theta]$ (as opposed to the r/η_θ normalization employed in figure 7). Using this non-dimensionalization, the data of figure 7 are re-plotted in figure 8, where it should be noted that the abscissa asymptotes to 0 as $r \to 2\pi\eta_\theta$ and to 1 as $r \to 2\pi\ell_\theta$. One immediately observes that the collapse of the kurtosis structure function data measured using different scalar-field boundary conditions improves significantly. (This normalization does not collapse the large-scale statistics, which will be expounded upon shortly.) This result may suggest that, when appropriately compensated for their different Péclet numbers, the scaling exponents of the two scalar fields are significantly less different. That being said, such a renormalization renders the estimation of scaling exponents more difficult, since well-defined power-law scaling regions are no longer observed. More importantly, however, this result supports the previous conclusion that the observed difference in the passive scalar structure function scaling exponents is related to the different Péclet numbers of the two scalar fields (i.e. the difference in their scalar integral length scales), and is not solely (if at all) a reflection of the relative levels of internal intermittency of the two passive scalar fields.

Like the passive scalar structure functions, the mixed sixth-order structure functions presented in figure 5 can also be normalized using the variance of the fluctuating velocity and passive scalar fields as follows:

$$\langle(\Delta_r u)^2\,(\Delta_r\theta)^4\rangle/(\langle(\Delta_r u)^2\rangle\langle(\Delta_r\theta)^2\rangle^2). \tag{3.4}$$

They then become ‘mixed sixth-order super-kurtosis structure functions’, which are presented in figure 9. Plotted in this manner, the mixed super-kurtosis structure functions for the different scalar fields achieve their respective asymptotic large-scale

https://doi.org/10.1017/jfm.2012.469 Published online by Cambridge University Press

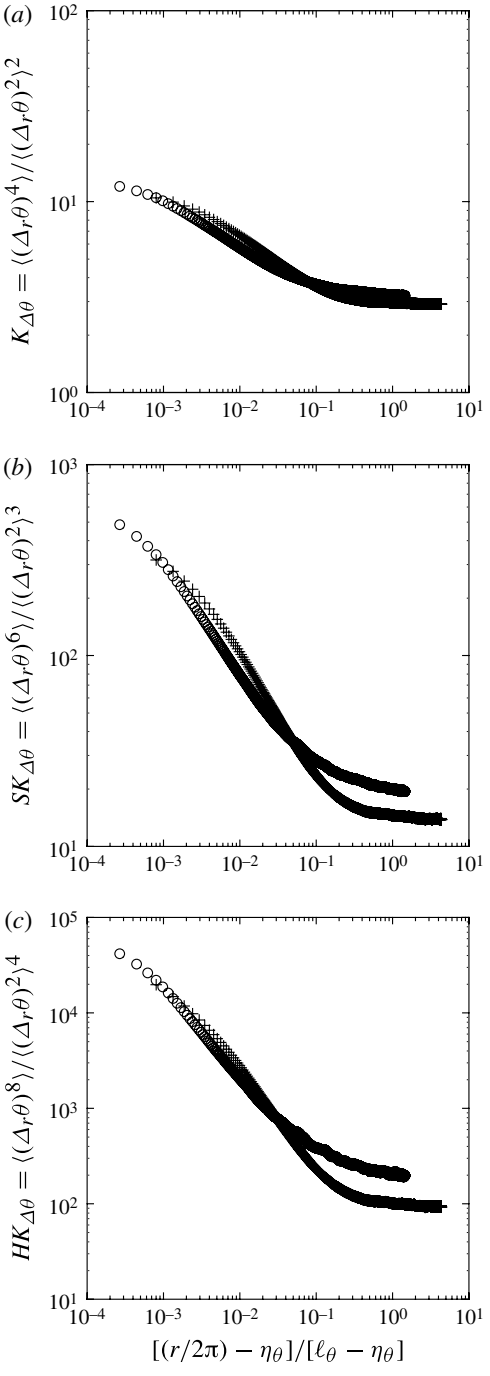


FIGURE 8. The kurtosis structure functions, $\langle(\Delta_r\theta)^n\rangle/\langle(\Delta_r\theta)^2\rangle^{n/2}$, plotted as a function of the Péclet-number-compensated separation ($[(r/2\pi) - \eta_\theta]/[\ell_\theta - \eta_\theta]$). (*a*) Kurtosis ($n = 4$); (*b*) super-kurtosis ($n = 6$); (*c*) hyper-kurtosis ($n = 8$). ∘, heated cylinder experiment; +, mandoline experiment.

https://doi.org/10.1017/jfm.2012.469 Published online by Cambridge University Press

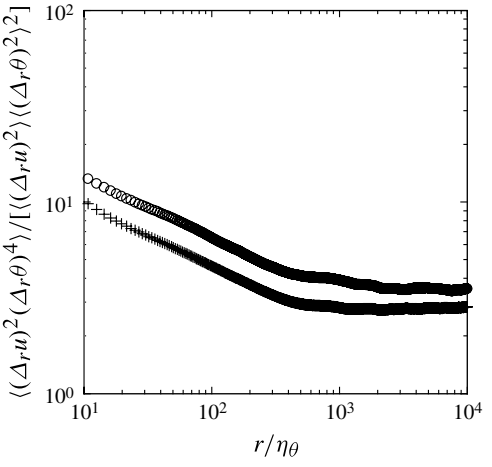


FIGURE 9. The mixed (i.e. velocity–temperature) 'super-kurtosis' (i.e. sixth-order) structure function, $\langle(\Delta_r u)^2\,(\Delta_r\theta)^4\rangle/(\langle(\Delta_r u)^2\rangle\,\langle(\Delta_r\theta)^2\rangle^2)$, plotted as a function of the separation, for the scalar fields generated by the heated cylinder and mandoline: ∘, heated cylinder experiment; +, mandoline experiment.

values at similar separations (which, as demonstrated in figure 7, was clearly not the case for the analogous passive scalar kurtosis structure functions). The fact that such mixed velocity–temperature structure functions are less dependent on their respective values of ℓ_θ (which are different for both flows) is consistent with the (grid-turbulence) results of Mydlarski (2003), who noted that mixed velocity-passive scalar (co-spectra and) structure functions resembled more closely those of the velocity field than those of the scalar field. This suggests that the reason the scaling exponents determined from the mixed velocity-passive scalar structure functions are similar and therefore not as Péclet-number-dependent is because these statistics are dominated by the velocity field, and therefore not as contaminated by the different large scales of the scalar field. (Recall that ℓ is the same for both flows.)

The autocorrelations of the dissipation rate of scalar variance, $\rho_{\chi\chi}(r)$, presented in figure 6, also exhibit a similar independence of the scalar-field boundary conditions. Since this statistic is an autocorrelation of a small-scale quantity (i.e. the dissipation rate of scalar variance), it is reasonable to expect that such a quantity would be less sensitive to the large-scale anisotropies of the temperature field.

It has been shown that the most commonly measured estimators of (passive scalar) internal intermittency – i.e. the high-order passive scalar structure function exponents – are Péclet-number-dependent, whereas measures of intermittency derived from either (i) autocorrelations of the scalar dissipation rate, or (ii) the mixed sixth-order structure functions appear to be effectively independent of Péclet number. Consequently, the dependence of different measures of intermittency on the Péclet number/boundary conditions is (i) of particular interest to any future work on this subject, and especially pertinent to any conclusions drawn pertaining to the degree(s) of universality of passive scalar fields, and (ii) possibly indicative of further differences between the hydrodynamic and scalar fields – differences which remain intriguing and not fully explained. Lastly, the question of which, if any, of the measures of internal intermittency studied herein is best and/or correct, remains open.

https://doi.org/10.1017/jfm.2012.469 Published online by Cambridge University Press

3.3. *Compensation of kurtosis structure functions*

We return to the previous observation that the large-scale heated cylinder statistics in figure 7 asymptote to constant values that are slightly larger than the analogous values for the mandoline statistics. Consequently, it is of interest to examine the effect of the large-scale asymptote of the kurtosis structure function (referred to as K_∞ herein) on the small-scale statistics (namely $K_{\Delta_r\theta}$). To this end, we propose the following two compensation techniques. Figure 10 plots the kurtosis structure functions, $K_{\Delta_r\theta}$, both offset (by subtraction), and normalized (by division) by their respective large-scale asymptotic values (i.e. K_∞): see figures 10(*a*,*c*,*e*) and 10(*b*,*d*,*f*), respectively. (As previously mentioned, $K_{\Delta_r\theta}$ will approach K_θ, the kurtosis of the fluctuating scalar field, in the limit of $r \to \infty$. In the present work, ℓ_θ for the mandoline experiment is sufficiently small that $K_\theta \approx K_\infty$, which is not the case for the heated cylinder experiment.) While there is no *a priori* reason to argue in favour of either technique, it must be noted that offsetting ($K_{\Delta_r\theta} - K_\infty$) preserves the interpretation of the kurtosis (since it represents a shift in the ordinate), whereas normalization ($K_{\Delta_r\theta}/K_\infty$) does not. (The interpretation of such a normalization is discussed below.) The offset kurtosis structure functions ($K_{\Delta_r\theta} - K_\infty$) presented in figure 10(*a*,*c*,*e*) reveal that the data obtained from the heated cylinder experiment exhibit a larger deviation from their asymptotic values than the analogous results from the mandoline experiment. Unfortunately, no conclusions pertaining to the intensity of the internal intermittency can be drawn from these data, since the magnitude of the kurtosis structure alone may depend upon flow-dependent, large-scale parameters.

Regarding the normalized kurtosis structure functions (i.e. $K_{\Delta_r\theta}/K_\infty$), one observes that, as required, the data asymptote to unity at large scales. Interestingly, one also observes a collapse of the data at small scales. However, the heated cylinder and mandoline statistics diverge at intermediate scales, with the magnitude of the divergence increasing with structure function order (and with the heated cylinder taking on larger values). While the current normalization successfully reconciles the small-scale statistics of the two different scalar fields, one must note that, as previously stated, the data normalized in this fashion are no longer physically representative of the kurtosis of the passive scalar field. Lastly, note that the data, when plotted as $K_{\Delta_r\theta}/K_\theta$ (not shown), collapse over a smaller extent but nevertheless also exhibit increasing divergence as the structure function order increases.

The divergence of the data in figure 10(*b*,*d*,*f*) at intermediate scales merits further discussion. To this end, we note that Schumacher, Sreenivasan & Yeung (2003) used nearby even-order moments to non-dimensionalize the odd-order statistics of the velocity gradient – e.g. $\langle x^5\rangle/\langle x^4\rangle^{5/4}$, $\langle x^5\rangle/\langle x^6\rangle^{5/6}$ and $\langle x^5\rangle/[\langle x^4\rangle\langle x^6\rangle]^{1/2}$, where x is the velocity gradient, $\partial u/\partial y$ – since normalization using the variance may not be valid in intermittent (i.e. non-Gaussian) phenomena. Warhaft & Gylfason (2004) examined various high-order statistics of the passive scalar increments in homogeneous, isotropic turbulence using the different non-dimensionalizations presented in Schumacher *et al.* (2003) to compensate for the effects of internal intermittency. Warhaft & Gylfason (2004) concluded that, while the normalizations proposed by Schumacher *et al.* (2003) were successful in compensating the low-order statistics, they simply delayed the effects of internal intermittency to higher-order statistics. Reasoning along these lines, combined with the observation that the magnitude of the difference between the heated cylinder and mandoline statistics at intermediate scales increases with the kurtosis structure function order, leads to the conclusion that this difference will eventually permeate to the small scales at higher orders. Consequently, although the present

https://doi.org/10.1017/jfm.2012.469 Published online by Cambridge University Press

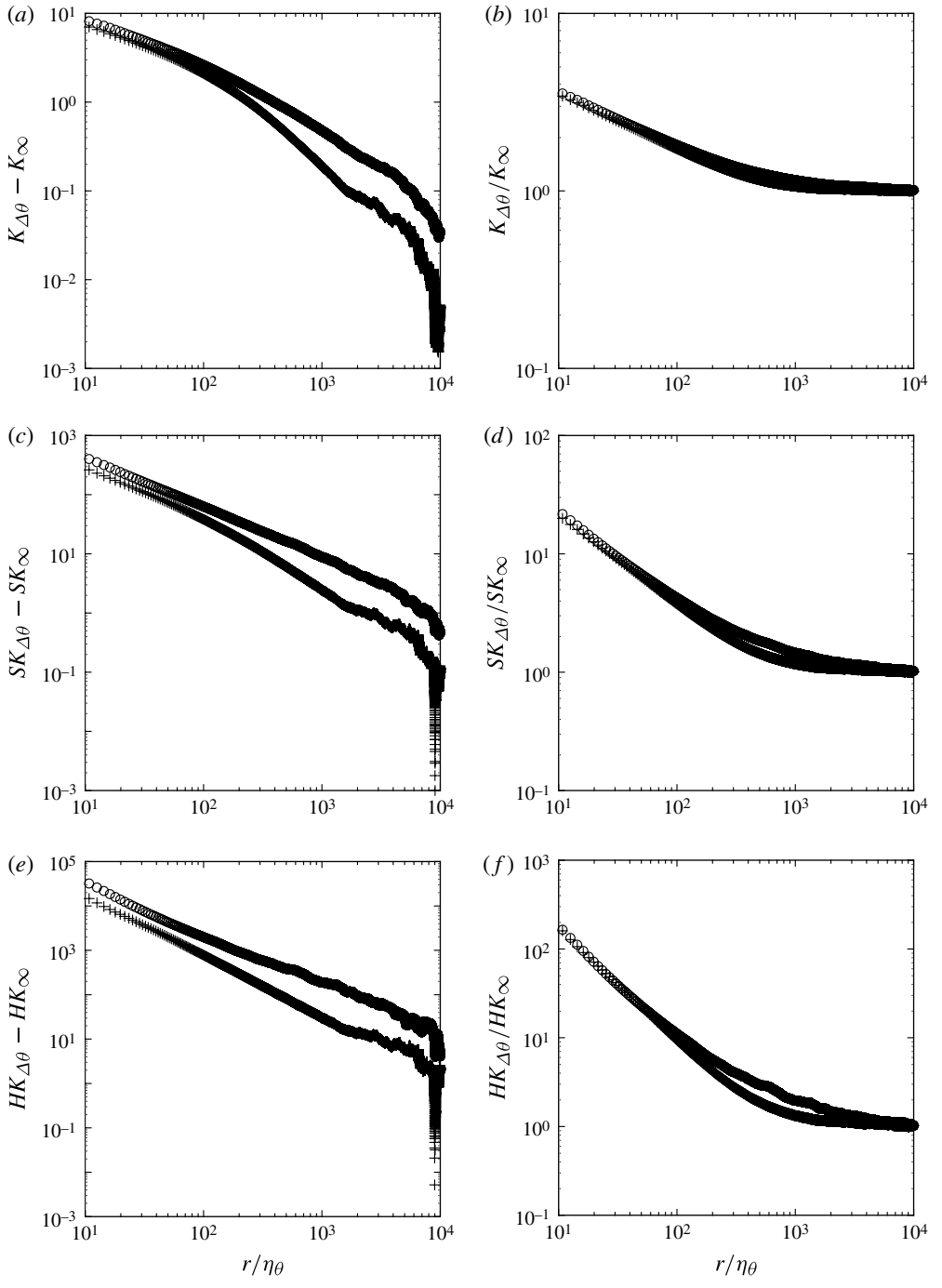


FIGURE 10. The offset and normalized kurtosis structure functions of the passive scalar increment ($K_{\Delta_r\theta} - K_\infty$ and $K_{\Delta_r\theta}/K_\infty$, respectively) plotted as a function of the separation (r/η_θ). (*a*,*c*,*e*) Offset kurtosis structure functions; (*b*,*d*,*f*) normalized kurtosis structure functions. (*a*,*b*) Kurtosis ($n = 4$); (*c*,*d*) super-kurtosis ($n = 6$); (*e*,*f*) hyper-kurtosis ($n = 8$). ∘, heated cylinder experiment; +, mandoline experiment.

https://doi.org/10.1017/jfm.2012.469 Published online by Cambridge University Press

normalization successfully collapses the small-scale data (particularly at low orders), the normalization employed in figure 10(*b*,*d*,*f*) delays the onset of the effects of internal intermittency to even higher-order statistics, consistent with the results of Warhaft & Gylfason (2004).

4. Conclusions

The influence of the scalar-field boundary conditions on the small-scale statistics of passive scalar increments were experimentally studied in the heated wake of a circular cylinder at a Taylor-microscale Reynolds number of 370. To explicitly isolate the influence of the scalar-field boundary conditions, two independent heat injection mechanisms were employed. However, the hydrodynamic field was identical for both cases. Results pertaining to the (i) high-order passive scalar structure functions (and their inertial-convective-range scaling exponents), (ii) mixed, velocity–temperature sixth-order structure functions, (iii) (non-centred) autocorrelations of the dissipation rate of scalar variance, and (iv) normalized high-order moments of the passive scalar increments were presented.

The second-order passive scalar structure functions obtained using the different scalar injection mechanisms were experimentally indistinguishable in the inertial-convective and dissipative ranges of scales. However, as the structure function order increased, the structure functions began to differ at progressively smaller scales. By eighth order, the curves were different at almost all scales. This result indicates that the effects of the different large scales permeate to the small scales at the highest orders. An analysis of the (inertial-convective-range) structure function scaling exponents showed that the structure function scaling exponents obtained using the different scalar-field boundary conditions (i) are significantly different from each other at high orders, and (ii) increasingly deviate from each other with increasing structure function order. This result is consistent with those obtained in the direct numerical simulation of Watanabe & Gotoh (2006), who also observed that different scalar sources yield different inertial-convective-range scaling exponents.

It was observed that the effects of the scalar-field boundary conditions were small and confined to the largest scales for low-order structure functions. However, the differences in the two scalar fields became more pronounced with increasing structure function order, with the scalar field generated by the mandoline exhibiting smaller inertial-convective-range scaling exponents. To further study these effects, and, more precisely, determine whether this result was truly indicative of the relative levels of the internal intermittency of the passive scalar fields examined herein, other statistics were considered.

The inertial-convective-range scaling exponents of both the mixed sixth-order structure functions and the autocorrelations of the dissipation rate of scalar variance were employed to obtain estimates of the intermittency exponent of the flows under consideration herein. Contrary to the result obtained from the passive scalar structure function scaling exponents, these latter two measures indicated that the scalar fields generated by the mandoline and by heating the cylinder have experimentally indistinguishable degrees of internal intermittency. Furthermore, the inertial-convective scaling ranges of these two quantities also exhibited a lack of dependence/sensitivity to the large scales of the flow. Whereas it has been shown that the (i) inertial-convective-range structure function scaling exponents are clearly affected by the large-scale features of the passive scalar field at high orders, and (ii) autocorrelations of the dissipation rate of scalar variance and the mixed sixth-order structure functions

https://doi.org/10.1017/jfm.2012.469 Published online by Cambridge University Press

are significantly less sensitive to the scalar-field boundary conditions, the question of which, if any, of these measures is the 'correct' estimator of passive scalar intermittency remains open.

In addition to the statistics described above, the kurtosis structure functions of the passive scalar increment were examined. For large separations, the high-order moments asymptoted to their respective large-scale, quasi-Gaussian values. However, at small scales, the moments deviated significantly from the Gaussian prediction, due to internal intermittency. Moreover, it was noted that the high-order moments of the mandoline data reached their large-scale, quasi-Gaussian values at smaller values of r/η_θ than their heated cylinder counterparts, due to the smaller scalar integral length scale of the mandoline-generated temperature field. Consequently, the inertial-convective-range, power-law slopes of the kurtosis structure functions for the mandoline data are steeper (i.e. have smaller/more negative scaling exponents) than the heated cylinder data. Since the slopes of the high-order moment curves are directly proportional to the structure function scaling exponents, it can be concluded that the scaling exponents for the mandoline experiment are anomalously smaller than those obtained from the heated cylinder experiment because of the smaller inertial-convective range in the former experiment, and are therefore not solely a reflection of a more intermittent passive scalar field, but remain affected by the smaller Péclet number of the scalar field generated by the mandoline.

In light of this result, the mixed, sixth-order structure functions described above were also non-dimensionalized using the variances of differences of the velocity and scalar fields to obtain a mixed 'super-kurtosis' structure function (analogous to the normalized high-order moments discussed in the previous paragraph). Plotting the mixed super-kurtosis structure functions revealed that the data obtained using the different scalar-field boundary conditions achieve their respective, large-scale asymptotic values at roughly the same separation, unlike the passive scalar structure functions.

The current results suggest that a direct relationship between the internal intermittency of the turbulent passive scalar and the inertial-convective-range scaling exponents of the high-order passive scalar structure functions can only exist when the inertial-convective ranges of the scalar fields are of the same width (or, alternately, infinite). Such a result is also consistent with previous works that have shown that large-scale effects such as non-stationarity (Danaila *et al.* 1999) or production (Danaila & Mydlarski 2001) contaminate the inertial-convective-range statistics. While the two flows examined herein have the same Reynolds number, their Péclet numbers are different because of the different thermal integral length scales associated with the different heat injection mechanisms. Consequently, the flows examined herein have the same inertial ranges, but different inertial-convective ranges.

To isolate the influence of the different scalar integral length scales, the kurtosis structure functions were plotted versus a Péclet-number-compensated separation. In doing so, one observes that the collapse of the kurtosis structure functions obtained using the different scalar-field boundary conditions improves at small scales.

Finally, the effects of large-scale anisotropy were examined by (i) offsetting, and (ii) normalizing the kurtosis structure functions by their respective, quasi-Gaussian, asymptotic values. (Note that the former preserves the interpretation of the kurtosis, whereas the latter does not.) Unfortunately, no conclusions pertaining to the passive scalar internal intermittency can be drawn from the offset kurtosis structure functions, since the magnitude of these statistics alone may be dependent upon large-scale, flow-dependent features. The normalized kurtosis structure functions exhibited a reasonable

https://doi.org/10.1017/jfm.2012.469 Published online by Cambridge University Press

collapse at both large and small scales, and diverge only at intermediate scales (with the magnitude of the divergence increasing with structure function order, and the heated cylinder flow taking on larger values). Since the observed difference in the kurtosis structure functions permeates to smaller scales with increasing structure function order, it is not unreasonable to assume that the data will no longer collapse at small scales at even higher orders.

Acknowledgements

The authors would like to thank the reviewers for their constructive comments, which served to improve the manuscript. The former also thank G. Tewfik, M. Iacobaccio and T. Micozzi for their superior technical assistance. Last, but not least, the authors gratefully acknowledge the generous continued support of the Natural Sciences and Engineering Research Council of Canada.

Appendix. Experimental conditions and flow validation

The following appendix serves to (i) characterize the hydrodynamic and thermal fields studied herein, and (ii) discuss potential sources of error.

The primary objective of this work is to examine the influence of the scalar-field boundary conditions on the small-scale statistics of the passive scalar field using the experimental configuration described in § 2. Therefore, the passive nature of the scalar (temperature) field must first be verified. Table 1 reveals that the r.m.s. temperature fluctuation obtained using either scalar-field boundary condition is considerably less than 1 °C. Consequently, the change in fluid density associated with such a small temperature change will be negligible, thus providing the first indication of a passive scalar field. To further confirm the passive nature of the temperature field, numerous statistics of the velocity field, including the p.d.f.s of the velocity fluctuation (figure 11*a*), the high-order velocity structure functions (figure 11*b*), and the spectra of turbulent kinetic energy (figure 11*c*), were computed for both the 'hot' (i.e. when the scalar source was energized) and 'cold' scenarios. Each of these statistics exhibited a collapse when plotted dimensionally (which is a more rigorous test than simply plotting them non-dimensionally), thereby confirming that the temperature field is indeed passive. As a final note, Berajeklian & Mydlarski (2011) recently presented mixed velocity–temperature statistics obtained under similar experimental conditions. They computed the ratio of buoyant production to the dissipation rate of turbulent kinetic energy and noted that this ratio did not exceed 2 % – another indication of a passive scalar field.

Given the objective stated above, it is also of utmost importance that the hydrodynamic flow field remains identical as the scalar injection mechanism is varied. To confirm this, the probability density functions (p.d.f.s) of the velocity fluctuation (see figure 11*a*) were computed when (i) only the cylinder was present in the wind tunnel and (ii) both the cylinder and mandoline were installed in the test section. The measured p.d.f.s exhibited a collapse over a range of ± 4 standard deviations, from which it was concluded that the presence of the mandoline has a negligible influence on the velocity field.

Kolmogorov theory applies to flows in which the scalar field is well mixed (and not 'externally intermittent'). Consequently, it is necessary to ensure that the scalar fields generated by the heated cylinder and mandoline are thoroughly mixed. This is accomplished by examining a variety of statistics, including the power spectra of the scalar fluctuations (see Lepore & Mydlarski 2009), in addition to the p.d.f.s

https://doi.org/10.1017/jfm.2012.469 Published online by Cambridge University Press

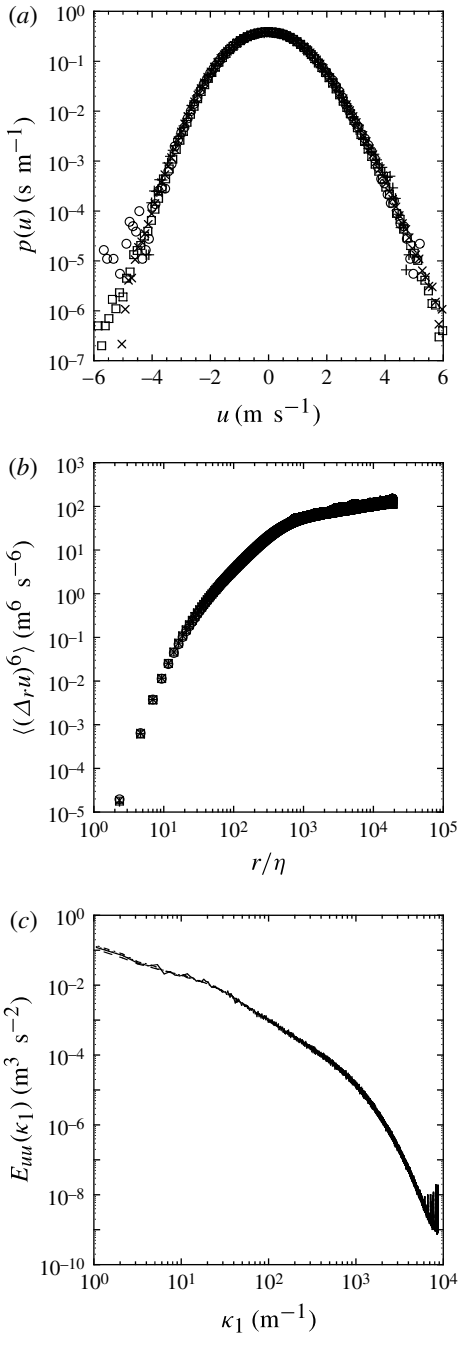


FIGURE 11. Comparison of the (*a*) p.d.f.s of the velocity fluctuation ($p(u)$), (*b*) sixth-order velocity structure functions ($\langle(\Delta_r u)^6\rangle$) and (*c*) power spectra of the velocity fluctuations ($E_{uu}(\kappa_1)$) for the different scalar-field boundary conditions, as well as for both the unheated and heated wakes. Note that the data are presented dimensionally. (*a*,*b*) ∘, unheated cylinder; +, unheated mandoline; □, heated cylinder; ×, heated mandoline. (*c*) Solid line, unheated cylinder; dashed line, unheated mandoline; dash-dotted line, heated cylinder; dotted line, heated mandoline.

https://doi.org/10.1017/jfm.2012.469 Published online by Cambridge University Press

of the temperature fluctuation (θ) (not shown). The measured temperature spectra demonstrate that the scalar fields differ at large scales (due to the different large-scale injection methods), thus yielding different p.d.f.s, as expected. In contrast to the p.d.f.s of the velocity field, there is no reason to assume that the scalar p.d.f.s will collapse. In fact, given the objectives of the present work, the p.d.f.s of the scalar fields must be different. Furthermore, the measured temperature spectra exhibit a collapse in the inertial-convective and dissipative ranges (as predicted by KOC theory), with an inertial-convective scaling region at least one decade in extent. The p.d.f.s of θ are smooth and unimodal, indicating that the wake is indeed well mixed. (A poorly mixed wake would exhibit a bimodal p.d.f., with a second sharp peak arising from unmixed fluid at the ambient temperature of the flow.) Consequently, the collapse of the scalar variance spectra at small scales, in addition to the smooth, unimodal p.d.f.s, supports the conclusion that the thermal wakes of both the heated cylinder and the mandoline are well mixed.

Computing the high-order moments of both the velocity and scalar fields requires measurement of the rare, intense fluctuations that occur within the flow. This information lies in the tails of the p.d.f., and thus requires sufficiently long data sets to accurately compute the high-order moments. Consequently, one must also verify that the high-order moments have indeed converged. This is accomplished by analysing fractions of the data set and comparing the results to those obtained from the full record. In addition to verifying that the statistics have converged, one must also verify that the higher-order moments are indeed closed. Examining the p.d.f.s of the scalar increments ($\Delta_r\theta$), and noting that:

$$\langle (\Delta_r\theta)^n \rangle \equiv \int_{-\infty}^{\infty} (\Delta_r\theta)^n \, p\,(\Delta_r\theta)\, \mathrm{d}(\Delta_r\theta), \tag{A 1}$$

the tails of the $(\Delta_r\theta)^n\, p\,(\Delta_r\theta)$ curve must go to zero as $\Delta_r\theta \to \pm\infty$ for the integral to close. Given the length of the data sets recorded herein, plots of $(\Delta_r\theta)^8\, p(\Delta_r\theta)\, \mathrm{d}(\Delta_r\theta)$ (see Lepore & Mydlarski 2009) reveal that the statistics have converged up to order $n = 8$. Anselmet *et al.* (1984) employed a similar technique to determine whether the higher-order moments measured therein were closed. However, they extrapolated the tails of their p.d.f.s to larger values of $\Delta_r u$ (by assuming an exponential form of the p.d.f. of $\Delta_r u$), and therefore extrapolated the integrand, to 'artificially' close the high-order moments. Anselmet *et al.* (1984) remarked that the measured value of $\langle (\Delta_r u)^{12} \rangle$ is 30 % smaller than the extrapolated value. Moreover, the authors discussed the validity of using such an extrapolation – in particular, they examined whether the p.d.f.s of $\Delta_r u$ will continue to decrease exponentially, or whether $\Delta_r u$ is bounded. Given these concerns, the present work does not employ any techniques that artificially close the higher-order moments.

REFERENCES

ANSELMET, F., ANTONIA, R. A. & DANAILA, L. 2001 Turbulent flows and intermittency in laboratory experiments. *Planet. Space Sci.* **49**, 1177–1191.

ANSELMET, F., GAGNE, Y., HOPFINGER, E. J. & ANTONIA, R. A. 1984 High-order velocity structure functions in turbulent shear flows. *J. Fluid Mech.* **140**, 63–89.

ANTONIA, R. A., HOPFINGER, E. J., GAGNE, Y. & ANSELMET, F. 1984 Temperature structure functions in turbulent shear flows. *Phys. Rev.* A **30**, 2704–2707.

ANTONIA, R. A., SATYAPRAKASH, B. R. & CHAMBERS, A. J. 1982 Reynolds number dependence of velocity structure functions in turbulent shear flows. *Phys. Fluids* **25**, 29–37.

https://doi.org/10.1017/jfm.2012.469 Published online by Cambridge University Press

ARNEODO, A., BAUDET, C., BELIN, F., BENZI, R., CASTAING, B., CHABAUD, B., CHAVARRIA, R., CILIBERTO, S., CAMUSSI, R., CHILLÀ, F., DUBRULLE, B., GAGNE, Y., HEBRAL, B., HERWEIJER, J., MARCHAND, M., MAURER, J., MUZY, J. F., NAERT, A., NOULLEZ, A., PEINKE, J., ROUX, F., TABELING, P., VAN DE WATER, W. & WILLAIME, H. 1996 Structure functions in turbulence, in various flow configurations, at Reynolds number between 30 and 5000, using extended self-similarity. *Europhys. Lett.* **34**, 411.

BEAULAC, S. & MYDLARSKI, L. 2004 Dependence on the initial conditions of scalar mixing in the turbulent wake of a circular cylinder. *Phys. Fluids* **16**, 3161–3172.

BELIN, F., TABELING, P. & WILLAIME, H. 1996 Exponents of the structure functions in a low temperature helium experiment. *Physica* D **93**, 52–63.

BENZI, R., CILIBERTO, S., BAUDET, C. & RUIZ CHAVARRIA, G. 1995 On the scaling of three-dimensional homogeneous and isotropic turbulence. *Physica* D **80**, 385–398.

BENZI, R., CILIBERTO, S., TRIPICCIONE, R., BAUDET, C., MASSAIOLI, F. & SUCCI, S. 1993 Extended self-similarity in turbulent flows. *Phys. Rev.* E **48**, R29–R32.

BERAJEKLIAN, A. & MYDLARSKI, L. 2011 Simultaneous velocity–temperature measurements in the heated wake of a cylinder with implications for the modelling of turbulent passive scalars. *Phys. Fluids* **23**, 055107.

BORATAV, O. N. & PELZ, R. B. 1997 Structures and structure functions in the inertial range of turbulence. *Phys. Fluids* **9**, 1400–1415.

BORATAV, O. N. & PELZ, R. B. 1998 Coupling between anomalous velocity and passive scalar increments in turbulence. *Phys. Fluids* **10**, 2122–2124.

CAMUSSI, R. & VERZICCO, R. 2000 Anomalous scaling exponents and coherent structures in high Re fluid turbulence. *Phys. Fluids* **12**, 676–687.

CAO, N. & CHEN, S. 1997 An intermittency model for passive-scalar turbulence. *Phys. Fluids* **9**, 1203–1205.

CHAMBERS, A. J. & ANTONIA, R. A. 1984 Atmospheric estimates of power-law exponents μ and μ_θ. *Boundary-Layer Meteorol.* **28** (3–4), 343–352.

CHEN, S. & CAO, N. 1997 Anomalous scaling and structure instability in three-dimensional passive scalar turbulence. *Phys. Rev. Lett.* **78**, 3459–3462.

CHEN, S. & KRAICHNAN, R. H. 1998 Simulations of a randomly advected passive scalar field. *Phys. Fluids* **10**, 2867–2884.

CORRSIN, S. 1951 On the spectrum of isotropic temperature fluctuations in an isotropic turbulence. *J. Appl. Phys.* **22**, 469–473.

DANAILA, L., ANSELMET, F., ZHOU, T. & ANTONIA, R. A. 1999 A generalization of Yaglom's equation which accounts for the large-scale forcing in heated decaying turbulence. *J. Fluid Mech.* **391**, 359–372.

DANAILA, L. & MYDLARSKI, L. 2001 Effect of gradient production on scalar fluctuations in decaying grid turbulence. *Phys. Rev.* E **64**, 016316.

DIMOTAKIS, P. E. 2005 Turbulent mixing. *Annu. Rev. Fluid Mech.* **37**, 329–356.

FRENKIEL, F. N. & KLEBANOFF, P. S. 1967 Higher-order correlations in a turbulent field. *Phys. Fluids* **10**, 507–520.

FRISCH, U. 1995 *Turbulence: The Legacy of A. N. Kolmogorov*. Cambridge University Press.

FRISCH, U., SULEM, P.-L. & NELKIN, M. 1978 A simple dynamical model of intermittent fully developed turbulence. *J. Fluid Mech.* **87**, 719–736.

GOTOH, T., FUKAYAMA, D. & NAKANO, T. 2002 Velocity field statistics in homogeneous steady turbulence obtained using a high-resolution direct numerical simulation. *Phys. Fluids* **14**, 1065–1081.

GYLFASON, A. & WARHAFT, Z. 2004 On higher order passive scalar structure functions in grid turbulence. *Phys. Fluids* **16**, 4012–4019.

HOLZER, M. & SIGGIA, E. D. 1994 Turbulent mixing of a passive scalar. *Phys. Fluids* **6**, 1820–1837.

JAYESH, TONG, C. & WARHAFT, Z. 1994 On temperature spectra in grid turbulence. *Phys. Fluids* **6**, 306–312.

KOLMOGOROV, A. N. 1941 The local structure of turbulence in incompressible viscous fluid for very large Reynolds numbers. *Dokl. Akad. Nauk SSSR* **30**, 301–305.

https://doi.org/10.1017/jfm.2012.469 Published online by Cambridge University Press

KRAICHNAN, R. H. 1994 Anomalous scaling of a randomly advected passive scalar. *Phys. Rev. Lett.* **72**, 1016–1019.

LARUE, J. C., DEATON, T. & GIBSON, C. H. 1975 Measurement of high-frequency turbulent temperature. *Rev. Sci. Instrum.* **46**, 757–764.

LEMAY, J. & BENAÏSSA, A. 2001 Improvement of cold-wire response for measurement of temperature dissipation. *Exp. Fluids* **31**, 347–356.

LEPORE, J. & MYDLARSKI, L. 2009 Effect of the scalar injection mechanism on passive scalar structure functions in a turbulent flow. *Phys. Rev. Lett.* **103**, 034501.

LÉVÊQUE, E., RUIZ-CHAVARRIA, G., BAUDET, C. & CILIBERTO, S. 1999 Scaling laws for the turbulent mixing of a passive scalar in the wake of a cylinder. *Phys. Fluids* **11**, 1869–1879.

LIENHARD, J. H. & HELLAND, K. N. 1989 An experimental analysis of fluctuating temperature measurements using hot-wires at different overheats. *Exp. Fluids* **7**, 265–270.

MAURER, J., TABELING, P. & ZOCCHI, G. 1994 Statistics of turbulence between two counterrotating disks in low-temperature helium gas. *Europhys. Lett.* **26**, 31–36.

MENEVEAU, C., SREENIVASAN, K. R., KAILASNATH, P. & FAN, M. S. 1990 Joint multifractal measures: theory and applications to turbulence. *Phys. Rev.* A **41**, 894–913.

MYDLARSKI, L 2003 Mixed velocity-passive scalar statistics in high-Reynolds-number turbulence. *J. Fluid Mech.* **475**, 173–203.

MYDLARSKI, L. & WARHAFT, Z. 1996 On the onset of high-Reynolds-number grid-generated wind tunnel turbulence. *J. Fluid Mech.* **320**, 331–368.

MYDLARSKI, L. & WARHAFT, Z. 1998 Passive scalar statistics in high-Péclet-number grid turbulence. *J. Fluid Mech.* **358**, 135–175.

OBOUKHOV, A. M. 1949 Structure of the temperature field in turbulent flows. *Izv. Akad. Nauk. SSSR Geogr. Geofiz* **13**, 58–69.

PRASAD, R. R., MENEVEAU, C. & SREENIVASAN, K. R. 1988 Multifractal nature of the dissipation field of passive scalars in fully turbulent flows. *Phys. Rev. Lett.* **61** (1), 74–77.

RUIZ CHAVARRIA, G., BAUDET, C. & CILIBERTO, S. 1995 Extended self-similarity of passive scalars in fully developed turbulence. *Europhys. Lett.* **32**, 319.

RUIZ-CHAVARRIA, G., BAUDET, C. & CILIBERTO, S. 1996 Scaling laws and dissipation scale of a passive scalar in fully developed turbulence. *Physica* D **99**, 369–380.

SCHMITT, F., SCHERTZER, D., LOVEJOY, S. & BRUNET, Y. 1996 Multifractal temperature and flux of temperature variance in fully developed turbulence. *Europhys. Lett.* **34** (3), 195–200.

SCHUMACHER, J., SREENIVASAN, K. R. & YEUNG, P. K. 2003 Derivative moments in turbulent shear flows. *Phys. Fluids* **15**, 84–90.

SHE, Z.-S. & LEVEQUE, E. 1994 Universal scaling laws in fully developed turbulence. *Phys. Rev. Lett.* **72**, 336–339.

SHRAIMAN, B. I. & SIGGIA, E. D. 2000 Scalar turbulence. *Nature* **405**, 639–646.

SREENIVASAN, K. R. 1991 On local isotropy of passive scalars in turbulent shear flows. *Proc. R. Soc. Lond.* A **434**, 165–182.

SREENIVASAN, K. R. & ANTONIA, R. A. 1997 The phenomenology of small-scale turbulence. *Annu. Rev. Fluid Mech.* **29**, 435–472.

SREENIVASAN, K. R., ANTONIA, R. A. & DANH, H. Q. 1977 Temperature dissipation fluctuations in a turbulent boundary layer. *Phys. Fluids* **20** (8), 1238–1249.

SREENIVASAN, K. R. & KAILASNATH, P. 1993 An update on the intermittency exponent in turbulence. *Phys. Fluids* **5**, 512–514.

STOLOVITZKY, G. & SREENIVASAN, K. R. 1993 Scaling of structure functions. *Phys. Rev.* E **48**, R33–R36.

VAN ATTA, C. W. & CHEN, W. Y. 1970 Structure functions of turbulence in the atmospheric boundary layer over the ocean. *J. Fluid Mech.* **44**, 145–159.

VAN ATTA, C. W. & PARK, J. 1972 Statistical self-similarity and inertial subrange turbulence. In *Statistical Models and Turbulence* (ed. M. Rosenblatt & C. W. Van Atta), *Lecture Notes in Physics,* vol. 12, pp. 402–426. Springer.

VINCENT, A. & MENEGUZZI, M. 1991 The spatial structure and statistical properties of homogeneous turbulence. *J. Fluid Mech.* **225**, 1–20.

https://doi.org/10.1017/jfm.2012.469 Published online by Cambridge University Press

WARHAFT, Z. 2000 Passive scalars in turbulent flows. *Annu. Rev. Fluid Mech.* **32**, 203–240.

WARHAFT, Z. & GYLFASON, A. 2004 Passive scalar fine scale structure: recent results and implications for the velocity field. In *Advances in Turbulence X* (ed. H. I. Andersson & P.-A. Krogstad), p. 801 CIMNE.

WARHAFT, Z. & LUMLEY, J. L. 1978 An experimental study of the decay of temperature fluctuations in grid-generated turbulence. *J. Fluid Mech.* **88**, 659–684.

WATANABE, T. & GOTOH, T. 2006 Intermittency in passive scalar turbulence under the uniform mean scalar gradient. *Phys. Fluids* **18** (5), 058105.

XU, G, ANTONIA, R. A. & RAJAGOPALAN, S 2000 Scaling of mixed longitudinal velocity–temperature structure functions. *Europhys. Lett.* **49** (4), 452–458.

YAGLOM, A. M. 1949 On the local structure of a temperature field in a turbulent flow. *Dokl. Akad. Nauk SSSR* **69**, 743–746.

ZUKAUSKAS, A. 1972 Heat transfer from tubes in crossflow. In *Advances in Heat Transfer* (ed. J. P. Hartnett & T. F. Irvine Jr), *Advances in Heat Transfer*, vol. 8. pp. 93–160. Elsevier.

https://doi.org/10.1017/jfm.2012.469 Published online by Cambridge University Press